

Modulation of exchange bias in Py/IrMn films by surface acoustic waves

Jie Dong(董洁), Shuai Mi(米帅), Meihong Liu(刘美宏), Huiliang Wu(吴辉亮), Jinxuan Shi(石金暄), Huifang Qiao(乔慧芳), Qian Zhao(赵乾), Teng-Fei Zhang(张腾飞), Chenbo Zhao(赵晨博), Jianbo Wang(王建波), and Qingfang Liu(刘青芳)

Citation: Chin. Phys. B, 2025, 34 (**8**): 088502. DOI: 10.1088/1674-1056/adce99
http://cpb.iphy.ac.cn; http://iopscience.iop.org/cpb

What follows is a list of articles you may be interested in

Control of the magnonic excitation under the joint mechanism of magnetostrictive effect and magnetocrystalline anisotropy

Saisai Yu(鱼赛赛), Junbo Liu(刘竣菠), and Hao Xiong(熊豪)
Chin. Phys. B, 2025, 34 (**6**): 068502. DOI: 10.1088/1674-1056/add67c

Influence of exchange bias on spin torque ferromagnetic resonance for quantification of spin-orbit torque efficiency

Qian Zhao(赵乾), Tengfei Zhang(张腾飞), Bin He(何斌), Zimu Li(李子木), Senfu Zhang(张森富), Guoqiang Yu(于国强), Jianbo Wang(王建波), Qingfang Liu(刘青芳), and Jinwu Wei(魏晋武)
Chin. Phys. B, 2024, 33 (**5**): 058502. DOI: 10.1088/1674-1056/ad2d55

Magnetoresistance effect in vertical NiFe/graphene/NiFe junctions

Pei-Sen Li(李裴森), Jun-Ping Peng(彭俊平), Yue-Guo Hu(胡悦国), Yan-Rui Guo(郭颜瑞), Wei-Cheng Qiu(邱伟成), Rui-Nan Wu(吴瑞楠), Meng-Chun Pan(潘孟春), Jia-Fei Hu(胡佳飞), Di-Xiang Chen(陈棣湘), and Qi Zhang(张琦)
Chin. Phys. B, 2022, 31 (**3**): 038502. DOI: 10.1088/1674-1056/ac192e

Room-temperature electric control of exchange bias effect in $CoO_{1-\delta}$/Co films using $Pb(Mg_{1/3}Nb_{2/3})_{0.7}Ti_{0.3}O_3$ (110) substrates

Xin Wen(闻馨), Rui Wu(吴锐), Wen-Yun Yang(杨文云), Chang-Sheng Wang(王常生), Shun-Quan Liu(刘顺荃), Jing-Zhi Han(韩景智), Jin-Bo Yang(杨金波)
Chin. Phys. B, 2020, 29 (**9**): 098503. DOI: 10.1088/1674-1056/aba611

Thermal resistance matrix representation of thermal effects and thermal design of microwave power HBTs with two-dimensional array layout

Rui Chen(陈蕊), Dong-Yue Jin(金冬月), Wan-Rong Zhang(张万荣), Li-Fan Wang(王利凡), Bin Guo(郭斌), Hu Chen(陈虎), Ling-Han Yin(殷凌寒), Xiao-Xue Jia(贾晓雪)
Chin. Phys. B, 2019, 28 (**9**): 098502. DOI: 10.1088/1674-1056/ab3436

Modulation of exchange bias in Py/IrMn films by surface acoustic waves

Jie Dong(董洁), Shuai Mi(米帅), Meihong Liu(刘美宏), Huiliang Wu(吴辉亮), Jinxuan Shi(石金暄), Huifang Qiao(乔慧芳), Qian Zhao(赵乾), Teng-Fei Zhang(张腾飞), Chenbo Zhao(赵晨博), Jianbo Wang(王建波), and Qingfang Liu(刘青芳)†

School of Physical Science and Technology, Lanzhou University, Lanzhou 730000, *China*

(Received 11 February 2025; revised manuscript received 1 April 2025; accepted manuscript online 21 April 2025)

We investigate the surface acoustic wave (SAW) modulation of the exchange bias field (H_{EB}) in Py/IrMn films deposited on $LiNbO_3$ substrates. We measured the anisotropic magnetoresistance (AMR) of the multilayer film when continuous SAW or pulsed SAW were applied and obtained H_{EB}. With continuous SAW, the H_{EB} decreases continuously with power. While in the case of pulsed SAW, the H_{EB} first decreases and then stabilizes. Compared to pulsed SAW, the thermal effects from the continuous SAW lead to the continuous decrease of H_{EB} at higher SAW power, which is verified by the measurement of H_{EB} at different temperatures and input currents. Furthermore, our results show that pulsed SAW can effectively avoid thermal effects. The decrease of H_{EB} at smaller power in both continuous and pulsed SAW is mainly due to the SAW-induced dynamic strain field, which leads to a small perturbation in the magnetic moment of the FM layer. Combined with the AMR values measured at different angles during the saturation field, we believe that the SAW-induced dynamic strain field causes a 15° angle between the magnetic moment and the easy axis. Our experiments provide a different approach to manipulating H_{EB}, opening up a potential avenue for future manipulation of antiferromagnetic moments.

Keywords: exchange bias, surface acoustic wave, anisotropic magnetoresistance, thermal effect

PACS: 85.70.Ec, 77.80.bn, 75.30.Gw

DOI: 10.1088/1674-1056/adce99 **CSTR:** 32038.14.CPB.adce99

1. Introduction

The development of information technology has put forward higher requirements on the technical level of data storage, and magnetic randomized memory (MRAM) has become a popular field of research in data storage with its advantages of fast storage speed, high density and high stability.[1,2] The successful application of the EB effect at the ferromagnetic/antiferromagnetic (FM/AFM) interface in memory cells has significantly contributed to the development of MRAM,[3–5] in which the modulation of the EB effect is especially important in the reading of the data.[6] In the previous research, the modulation of the EB is mainly concerned with the stress,[7,8] voltage,[9–12] magnetic field cooling,[13–15] large pulsed magnetic field,[16,17] the helicity of optical,[18,19] single femtosecond laser pulse,[20] and in recent years, the spin–orbit torque (SOT) effect,[21–25] and so on. However, conventional methods have some limitations, for example, pulsed magnetic field control of EB is very power consuming, and SOT manipulation of EB presupposes that the sample has strong spin–orbit coupling or a large spin-Hall angle.[26]

SAW is an acoustic wave that propagates on the surface of the crystal.[27] Using SAW to manipulate the properties not only combines the low energy consumption of stress modulation with the convenience of SOT modulation, but also has lower requirements for film size (anywhere from nanometer to centimeter). It has been reported that SAW can assist the flipping of magnetic moments in the ferromagnetic films,[28–34] therefore, we hypothesize that SAW can also influence the arrangement of the magnetic moments in the interface of the FM/AFM and thus modulate the H_{EB}.

In this paper, the effects of continuous and pulsed SAW on H_{EB} in Py/IrMn thin films prepared on $LiNbO_3$ single-crystal substrates are investigated. The results show that the H_{EB} of the samples decreases with the increase of the continuous SAW input power, while the H_{EB} first decreases and then stabilizes under pulsed SAW.[32] Together with the changes of Hall resistance of the samples, it can be inferred that the effect of continuous SAW on H_{EB} is the combined effect of dynamic strain field and thermal effect, while pulsed SAW can effectively avoid the influence of the thermal effect.

2. Experimental methods

The multilayer film Ta(10 nm)/Py(10 nm)/IrMn(6 nm)/Ta (5 nm) are deposited on 128° Y-cut $LiNbO_3$ single crystal substrates by DC magnetron sputtering in 0.3 Pa of Ar, and the base pressure for sputtering is less than 1×10^{-5} Pa. The bottom 10-nm Ta layer is used as a seed layer to improve the growth quality and adhesion of the film, and the top layer of 5-nm Ta is used as a protective layer to prevent the film from

†Corresponding author. E-mail: liuqf@lzu.edu.cn

© 2025 Chinese Physical Society and IOP Publishing Ltd. All rights, including for text and data mining, AI training, and similar technologies, are reserved.

oxidizing. An in-plane magnetic field (H_s) with a magnitude of about 200 Oe (1 Oe = 79.5775 A·m^{-1}) was applied during the deposition process. This is done to induce the generation of an initial exchange bias. The direction of this deposition field is shown by the red arrow in Fig. 1(c), which is in the same direction as the current and magnetic field applied during the test and is perpendicular to the direction of acoustic wave transmission. Our SAW devices are fabricated on the substrate by the ultrahigh-vacuum room temperature DC magnetron sputtering technology and the lift-off process of the micro-nano processing technology. Figure 1(a) shows a simple schematic of the device. The gray area is a sample strip 600-μm long and 20-μm wide in size. The orange part of the figure shows the surface acoustic wave device as well as the electrode structure in the form of a Hall bar, which is made of Ta(5 nm)/Al(50 nm)/ Ta(5 nm). Port 1 and port 2 represent the input port and output port of the interdigital transducer (IDT) respectively. A locally enlarged schematic of the IDT is shown in the upper left corner of Fig. 1(a) with $P = 16$ μm, $\omega_1 = \omega_2 = 4$ μm, $L = 150$ μm, where P, ω_1, and ω_2 represent the period, finger width, and the gap of the IDT, L is the length of the IDT overlap, respectively. The physical diagram of the SAW device is shown in Fig. S1 in supporting information. We fix the SAW device on the printed circuit board, input the microwave signal through the SubMiniature version A(SMA) connector to excite the SAW. The blue arrow in Fig. 1(c) represents the direction of the wave vector of the SAW ($\boldsymbol{k}_{\mathrm{SAW}}$). The direction of the wave vector of the acoustic wave is determined by the crystal orientation of $LiNbO_3$. The acoustic waves excited in our prepared devices are narrow linewidth, high intensity Rayleigh waves. The red arrow indicates the direction of the current passed through and the direction of the magnetic field applied during the measurement. In our facility, we use a current source (Keithley 6221 DC and AC) and a nanovoltmeter (Keithley 2182A) to provide current and detect voltage. Field variants and data acquisition are automated using LabVIEW-based programs. It is well known that the effect of exchange anisotropy can be observed by measuring the anisotropic magnetoresistance (AMR). Therefore, we measure the AMR of the films using the four-probe method to obtain the EB field. As shown in Fig. 1(a), a current of 0.5 mA is passed through ports 2 and 5 of the Hall bar, and the voltage values are measured at ports 1 and 4 to finally obtain the resistance $R = U/I$. During the measurement, the magnetic field is parallel to the direction of the current. The left and right IDTs are mirror symmetric, and the finger width and gap of the IDTs determine the wavelength (λ_{SAW}) of the SAW, which is equal to the period, i.e., $P = \lambda_{\mathrm{SAW}} = 2(\omega_1 + \omega_2)$. The penetration depth of SAW in $LiNbO_3$ is about one wavelength, and the thickness of our film is on the order of nanometers, so the entire film can be covered by sound waves. When the period of the IDT is kept constant, the eigenfrequency (f_0) of the SAW is a constant value. Odd harmonics may also occur during excitation of the surface acoustic wave at $f = nf_0$, n refers to the number of odd harmonics. Figure 1(b) shows the acoustic wave signal with the frequency of fundamental (1st), third harmonics (3rd), and fifth harmonics (5th) measured using the vector network analyzer (VNA). The fifth harmonic (5th) is selected for study in this work.

Due to a number of factors such as impedance, dissipation, and reflection, the actual acoustic SAW power acting on the sample is $P_a = \frac{1}{2}k^2\Delta|S_{11}|^2P$,[31,35] for $LiNbO_3$ substrates, the electromechanical coupling coefficient $k^2 = 5\%$ and P is the input power of the microwave source used to excite the acoustic SAW.[35,36]

The heating part of the experiment was done by taping the samples to our homemade heating device. The heater is used to control and change the temperature. Measurements are taken after the temperature has stabilized.

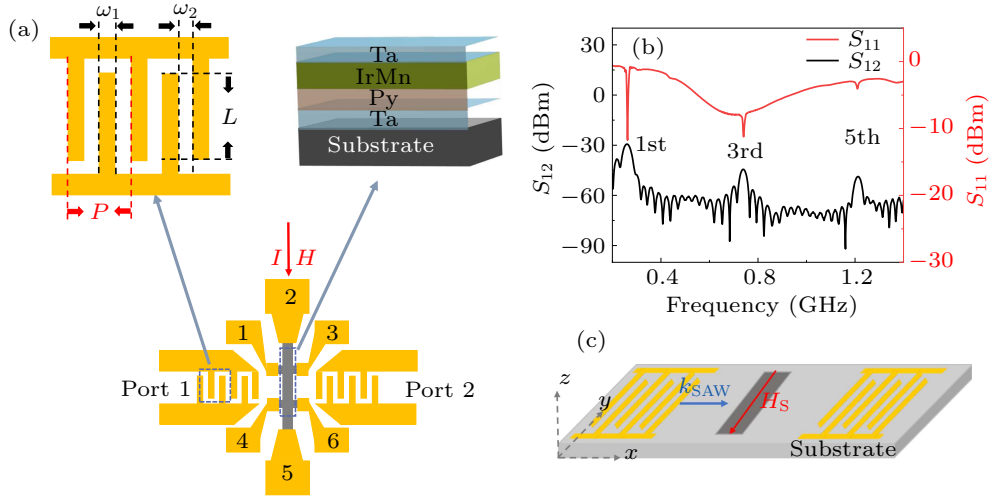


Fig. 1. (a) Simple schematic diagram of the SAW device. The partially enlarged IDT schematic and sequentially deposited Ta (10 nm)/Py (10 nm)/IrMn (6 nm)/Ta (5 nm) magnetic multilayers (not to scale) are shown in the upper left and right corners, respectively. (b) The reflection parameter S_{11} and the transmission parameter S_{12} of the SAW device. (c) Schematic diagram of SAW vector *versus* crystal orientation of $LiNbO_3$ substrate.

3. Result and discussion

In order to know how SAW modulate the exchange bias field, we prepared the device shown in Fig. 1(a). The direction of the SAW is perpendicular to the direction of the current and the external magnetic field. To exclude training effect, all results in our work are obtained by averaging 3 measurements. Here we apply a continuous SAW. The unit of power, dBm, is converted to mW as follows:

$$Y(\mathrm{dBm}) = 10\lg[X(\mathrm{mW})/1(\mathrm{mW})]. \tag{1}$$

We defined the intersection of the two blue and orange curves as the H_{EB}.[37] From Fig. 2(a), it can be seen that, without SAW applied, the base magnetoresistance value of the film is 87.85 Ω, the value of H_{EB} is −206.8 Oe. When the output power of the microwave source is increased to 10 dBm, the base resistance value of the film starts to rise, the value of H_{EB} is reduced to −188 Oe. When the power reaches 27 dBm, the resistance value of the film rises to 90.44 Ω, the value of H_{EB} decreased to −161.2 Oe, and the magnetoresistance curve is not closed at higher magnetic field. The magnetic field we applied was first along the orange solid curve from +600 Oe to −600 Oe then along the blue hollow curve from −600 Oe back to +600 Oe. Figure 2(b) plots the variation of H_{EB} with continuous SAW power. It shows that H_{EB} decreases with increasing SAW power. As the power of the SAW increases from 0 to 10 mW, the H_{EB} decreases rapidly along the linearity, the decrease slows down in the range of 10 mW–500 mW. And the H_{EB} still tends to decrease with the increase of power. This result suggests that the SAW has a role in modulating the exchange bias field. The hysteresis loop diagram of the sample is shown in Fig. S2.

To explain the experimental result we consider the Meiklejohn–Bean (MB) model. The expression for the exchange bias field in the MB model is

$$H_{\mathrm{EB}} \propto -\frac{J_{\mathrm{ex}}}{M_{\mathrm{FM}} t_{\mathrm{FM}}}, \tag{2}$$

where J_{ex} is the FM/AFM interfacial exchange coupling energy per unit area, M_{FM} is the magnetization of FM layer, t_{FM} is the thickness of FM layer. The expression of J_{ex} is as follows:[38,39]

$$J_{\mathrm{ex}} = nAS_{\mathrm{FM}}S_{\mathrm{AFM}}\cos\varphi, \tag{3}$$

where n is the uncompensated magnetic moment density at the interface, A is the exchange coupling constant of FM/AFM, S_{FM} and S_{AFM} are the spins of FM and AFM at the interface, respectively, and φ is the angle between the FM spin and AFM spin at the interface.

As the SAW is excited from the IDT, the dynamic strain field brought about by the propagation of the SAW on the $LiNbO_3$ substrate will be transferred to the magnetic multilayer film. Some experimental studies have shown that when the FM layer is very thin (i.e., the transverse dimension is much larger than the thickness), the strain is maximal in the ε_{xx} direction.[34] Therefore, when the ferromagnetic magnetic moment is subjected to tensile stress (compressive strain), it will deviate from the easy magnetization axis, resulting in an angle between the magnetic moment and the direction of the external field.[10,28] The reason for the H_{EB} reduction can be considered in terms of the interfacial exchange coupling energy of the FM/AFM. From Eqs. (2) and (3), it can be seen that when the magnetic moment of the FM layer deviates from the easy magnetization axis, the increase of φ leads to the decrease of J_{ex}, which in turn leads to the decrease of H_{EB}. The SAW excites a dynamic strain field on the $LiNbO_3$ substrate, which can be transferred to the immediately neighboring magnetic material. This involves a variety of mechanisms, including magneto-elastic coupling,[31,40] magneto-rotation coupling (MRC),[41] spin-rotation coupling (SRC),[42] and gyromagnetic coupling (GMC).[43] We speculate that it is the result of a combination of one or more of these mechanisms.[44]

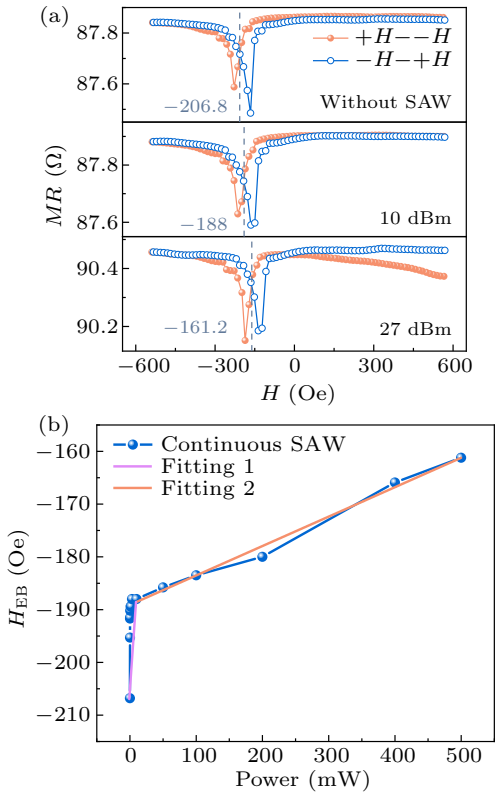


Fig. 2. (a) Variation of AMR of multilayer films with external magnetic field at different SAW powers. (b) Trend of H_{EB} values at different SAW powers.

In addition, we speculate that SAW has an effect not only on the FM layer but also on the AFM layer.[45] The dynamic strain field brought by the SAW will periodically modulate the magnetocrystalline anisotropy energy of the AFM, and when the magnetocrystalline anisotropy energy of the AFM goes to

a lower position, the pinning effect of the AFM on the FM is weakened, which is ultimately manifested in the reduction of the exchange bias field.

Not only that, but from Fig. 2, we can also see that as the power of the SAW rises, the value of our measured AMR also rises, as shown in Fig. 3. When the power of the SAW is small (0 mW–10 mW), the value of the magnetoresistance remains almost constant, while when the power of the SAW increases (10 mW–500 mW), the value of the magnetoresistance also increases gradually. We speculate that there is a thermal effect embedded in this. Regarding the source of the thermal effect, we speculate that it comes from the following two contributions: one from the input current during the measurement and the other from the high frequency SAW.

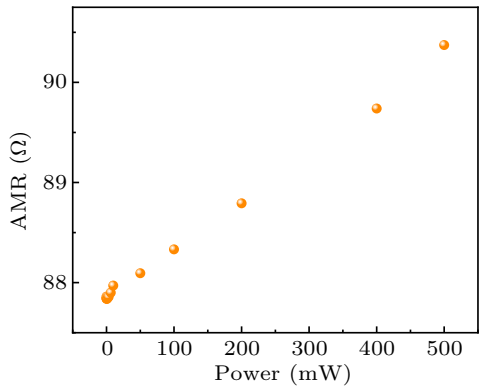


Fig. 3. Variation of the value of AMR with power in continuous SAW.

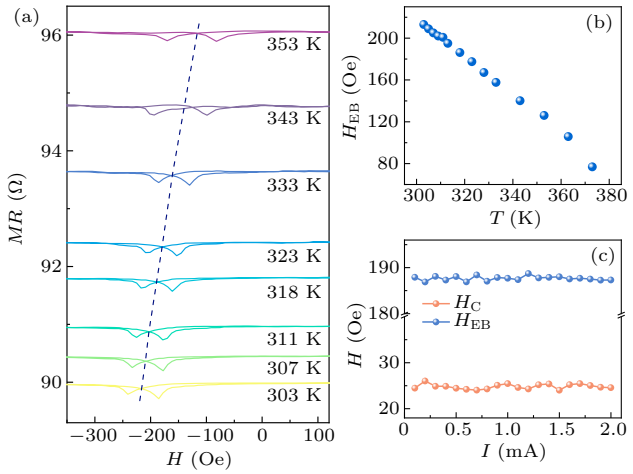


Fig. 4. (a) *MR*–*H* curves at different test temperatures. (b) Variation curve of H_{EB} with temperature. (c) Values of H_{EB} and H_C at different input currents.

To further explore the effect of thermal effect on H_{EB}, we measured the *MR*–*H* curves at different temperatures and the input currents. No SAW is applied during the measurements. As shown in Figs. 4(a) and 4(b), the value of AMR is increasing with increasing temperature and H_{EB} decreases linearly with temperature. When the value of AMR increases by 2.6 Ω, the corresponding H_{EB} decreases by 30 Oe. In addition to this, we also take into account the thermal effect of the current. According to Fig. 4(c), the H_{EB} hardly changes when the current increases from 0.1 A to 2 A. And in the above experiment, the current passed is 0.5 A, so we think that the thermal effect from the current is not enough to affect the size of H_{EB}. Combined with Fig. 2(a), the overall decrease in H_{EB} is 45.6 Oe when the AMR is elevated by 2.6 Ω. So after excluding the thermal effect from current and temperature, the remaining decrease of H_{EB} is due to the contribution from strain field of the SAW.

Therefore, to effectively avoid thermal effects, we use pulsed SAW to investigates the influence of dynamic strain field to H_{EB}. The pulse period used to excite the SAW was 50 ms with a pulse width of 10 μs.

Figure 5(a) shows a plot of the value of AMR as a function of magnetic field. When the power of the pulsed SAW is increased from −0.002 dBm to 0.0054 dBm, the value of H_{EB} decreases from −205.6 Oe to −194.1 Oe and there is an overall small decrease in the value of AMR. Figure 5(b) shows the variation of H_{EB} with SAW power. When the power of the pulsed SAW is in the range of 0 mW–10 mW, the H_{EB} decreases linearly and then slows down gradually. It remains stable when it reaches 200 mW and does not continue to decrease with increasing power. Therefore, when pulsed SAW is applied, the value of AMR does not rise, and we believe that the thermal effect can be effectively suppressed. In addition, there is a slight overall decrease in AMR, which we attribute to the slight deflection of the magnetic moments at the interface, which creates an angle between the magnetic moment of the ferromagnetic layer and the easy axis. Figure 5(c) exhibits the variation curve of AMR with pulsed SAW power in saturated magnetic field. It has a similar trend to H_{EB}. It decreases linearly at 0 mW–10 mW, after which the decrease slows down and stabilizes when it reaches 200 mW. Figure 5(d) shows the AMR at different θ measured at saturated magnetic field when no SAW is applied. θ is the angle between the magnetic field applied and the current passed. In Fig. 5(c), we can see that the value of AMR has decreased by 0.06 Ω. Combined with Fig. 5(d), we speculate that the magnetic moment of the FM layer has been deflected by approximately 15°. Without applying SAW, when $\theta = 0°$, H_{EB} equals −206.8 Oe, which can be calculated according to Eqs. (2) and (3), and when $\theta = 15°$, H_{EB} equals to −195.1 Oe, which is basically the same as our experimental results. This is what causes the H_{EB} to decrease.

The effect on coercivity is not significant for either continuous or pulsed SAW. The experimental results are shown in Fig. S3. We also measured the effect of the first and third harmonics on the H_{EB} when a pulsed SAW is applied. There is no significant trend in H_{EB} and MR at these two frequencies. This indicates that neither the first nor the third harmonic modulates the H_{EB}. Although the conversion efficiency decreases with increasing frequency, the energy density rises and the energy becomes more concentrated. This may be the reason why H_{EB} and MR are regulated by the SAW at the 5th harmonic, while the 1st and 3rd harmonics are not. The experimental results are shown in Figs. S4–S6.

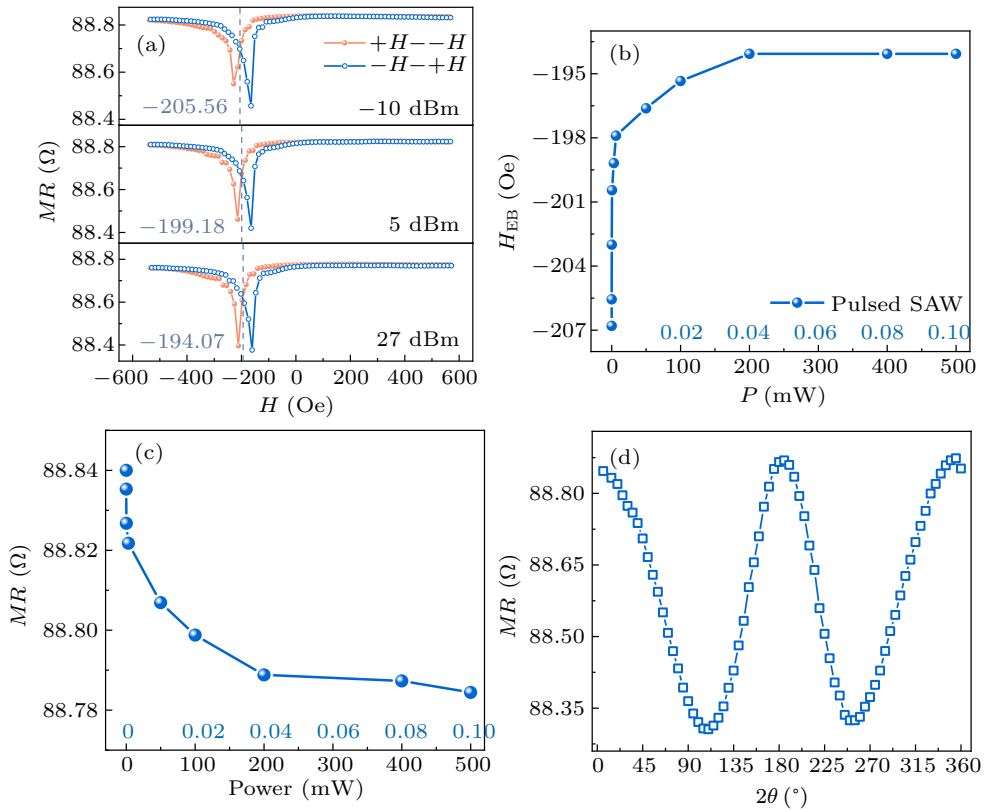


Fig. 5. (a) *MR*–*H* curves for different pulsed SAW powers applied. (b) Variation of exchange bias field with pulsed SAW power in multilayers. The blue numbers above the *x*-axis are time-averaged power. (c) Curve of AMR *versus* pulsed SAW power in saturated magnetic field. The blue numbers above the *x*-axis are time-averaged power. (d) Curve of AMR value with θ for saturated magnetic field. θ is the angle between the magnetic field applied during the measurement and the passed current.

It should also be noted that the change in H_{EB} for the SAW manipulation in this experiment is not significant. In previous experimental results, the modulation range of H_{EB} can be as high as 60% when continuous SAW is applied.[32] Of course, we think most of the contribution is from the thermal effects. To further improve the tuning range of EB in FM/AFM, two aspects can be considered in future experiments. Select FM materials with high magnetostriction coefficients, such as FeGa,[46] Ni, and so on. Select AFM materials with stronger strain response, such as Mn_2Au[47] and FeRh.[48] The finger width of the IDT in the SAW devices in our experiments is on the order of micrometers, which puts the wavelength of the SAW in the micrometer range. In fact, the wavelength of the SAW can reach the nanometer scale by increasing the process limit of lithography. It has been reported that the finger width and gap of IDTs can reach 35 nm, and the corresponding SAW fundamental frequency signal is close to 30 GHz, while the fundamental frequency wavelength of SAWs is only 160 nm,[49] a value comparable to the size of magnetic random memories (MRAM). The wavelength of SAWs can also be greatly shortened by exciting higher harmonics. It has been reported that the 13rd harmonic signal of the SAW is excited on an $LiNbO_3$ substrate, and the 13rd harmonic wavelength of the SAW can be calculated from the equation $v = f_0\lambda$ to reach the nanometer scale as well,[50] which means that the wavelength of the SAW can be fabricated and manipulated to be comparable to the size of the MRAM, and therefore, the manipulation of the MRAM with the SAW is feasible.

4. Conclusions

In summary, we investigated the effect of SAW on H_{EB} of Py/IrMn thin films. The experimental results show that the H_{EB} value decreases with the increase of SAW power in multilayer films. We mainly consider the magnetoelastic coupling effect as well as the AFM lattice vibration. The strain transfer of the SAW acting on the $LiNbO_3$ substrate into the magnetic film changes the spin structure at the FM/AFM interface, leading to the weakening of the exchange coupling energy at the FM/AFM interface, the weakening of the magnetocrystalline anisotropy of the AFM, and ultimately the reduction of the H_{EB}. In addition, we explore the effect of thermal effects on H_{EB}. Our work realizes the manipulation of H_{EB} by SAW, which provides a potential means for spin orientation control of AFM.

Acknowledgements

Project supported by the National Natural Science Foundation of China (Grant Nos. 12174166 and 12304144), the

Fund from Beijing National Laboratory for Condensed Matter Physics (Grant No. 2024BNLCMPKF013), and the Fundamental Research Funds for the Central Universities (Grant No. lzujbky-2024-22).

References

[1] Xu X, Hu W, Jia Y, Huang Y, Shan X, Zhu G, Ren H, He Q, Guo Q and Yu G 2024 *J. Phys. D: Appl. Phys.* **57** 225003
[2] Cai K, Jin T and Lew W S 2024 *Natl. Sci. Rev.* **11** nwad272
[3] Nogués J, Sort J, Langlais V, Skumryev V, Suriñach S, Muñoz J S and Baró M D 2005 *Phys. Rep.* **422** 65
[4] Ehrmann T B A 2021 *Coatings* **11** 122
[5] Blachowicz T, Ehrmann A and Wortmann M 2023 *Nanomaterials-Basel* **13** 2418
[6] Li H, Pan S, Wang Z, Xiang B and Zhu W 2024 *Chin. Phys. B* **33** 017504
[7] Zhang Z, Liu E, Zhang W, Wong P K J, Xu Z, Hu F, Li X, Tang J, Wee A T S and Xu F 2019 *ACS Appl. Mater. Interfaces* **11** 8258
[8] Sheng P, Xie Y, Bai Y, Wang B, Zhang L, Wen X, Yang H, Chen X, Li X and Li R W 2019 *Appl. Phys. Lett.* **115** 242403
[9] Rizwan S, Yu G Q, Zhang S, Zhao Y G and Han X F 2012 *J. Appl. Phys.* **112** 064120
[10] Polisetty S, Echtenkamp W, Jones K, He X, Sahoo S and Binek C 2010 *Phys. Rev. B* **82** 134419
[11] Zhai K, Chai Y, Cong J, Shang D and Sun Y 2018 *Phys. Rev. B* **98** 144405
[12] Holanda J, Saglam H, Karakas V, Zang Z, Li Y, Divan R, Liu Y, Ozatay O, Novosad V, Pearson J E and Hoffmann A 2020 *Phys. Rev. Lett.* **124** 087204
[13] Deng Z, Wang X, Wang M, *et al.* 2023 *Adv. Mater.* **35** 2209759
[14] Chen J Y, Thiyagarajah N, Xu H J and Coey J M D 2014 *Appl. Phys. Lett.* **104** 152405
[15] Kumar R, Sarangi S N, Samal D and Hossain Z 2021 *Phys. Rev. B* **103** 064421
[16] Nogués J, Sort J, Suriñach S, Muñoz J S, Baró M D, Bobo J F, Lüders U, Haanappel E, Fitzsimmons M R, Hoffmann A and Cai J W 2003 *Appl. Phys. Lett.* **82** 3044
[17] Shiratsuchi Y, Wakatsu K, Nakamura T, Oikawa H, Maenou S, Narumi Y, Tazoe K, Mitsumata C, Kinoshita T, Nojiri H and Nakatani R 2012 *Appl. Phys. Lett.* **100** 262413
[18] Vallobra P, Fache T, Xu Y, Zhang L, Malinowski G, Hehn M, Rojas-Sánchez J C, Fullerton E E and Mangin S 2017 *Phys. Rev. B* **96** 144403
[19] Chatterjee J, Polley D, Pattabi A, Jang H, Salahuddin S and Bokor J 2022 *Adv. Funct. Mater.* **32** 2107490
[20] Guo Z, Malinowski G, Vallobra P, Peng Y, Xu Y, Mangin S, Zhao W, Hehn M and Zhang B 2023 *Chin. Phys. B* **32** 087507
[21] Peng S, Zhu D, Li W, Wu H, Grutter A J, Gilbert D A, Lu J, Xiong D, Cai W, Shafer P, Wang K L and Zhao W 2020 *Nat. Electron.* **3** 757
[22] Lin P H, Yang B Y, Tsai M H, Chen P C, Huang K F, Lin H H and Lai C H 2019 *Nat. Mater.* **18** 335
[23] Zhou Z P, Liu X H and Wang K Y 2020 *Appl. Phys. Lett.* **116** 062403
[24] Saglam H, Rojas-Sanchez J C, Petit S, Hehn M, Zhang W, Pearson J E, Mangin S and Hoffmann A 2018 *Phys. Rev. B* **98** 094407
[25] Zhao Q, Zhang T, He B, Li Z, Zhang S, Yu G, Wang J, Liu Q and Wei J 2024 *Chin. Phys. B* **33** 058502
[26] Holanda J, Maior D S, Santos O A, Azevedo A and Rezende S M 2021 *Appl. Phys. Lett.* **118** 022409
[27] Holanda J, Maior D S, Azevedo A and Rezende S M 2018 *Nat. Phys.* **14** 500
[28] Davis S, Baruth A and Adenwalla S 2010 *Appl. Phys. Lett.* **97** 232507
[29] Thevenard L, Camara I S, Majrab S, Bernard M, Rovillain P, Lemaître A, Gourdon C and Duquesne J Y 2016 *Phys. Rev. B* **93** 134430
[30] Thevenard L, Camara I S, Prieur J Y, Rovillain P, Lemaître A, Gourdon C and Duquesne J Y 2016 *Phys. Rev. B* **93** 140405
[31] Cao Y, Bian X N, Yan Z, Xi L, Lei N, Qiao L, Si M S, Cao J W, Yang D Z and Xue D S 2021 *Appl. Phys. Lett.* **119** 012401
[32] Qiao H, Niu Y, Li X, Mi S, Liu X, Xue J, Wu S, Wang X, Liu Q and Wang J 2022 *J. Phys. D: Appl. Phys.* **56** 025003
[33] Schell V, Spetzler E, Wolff N, Bumke L, Kienle L, McCord J, Quandt E and Meyners D 2023 *Sci. Rep.* **13** 8446
[34] Seemann K M, Gomonay O, Mokrousov Y, Hörner A, Valencia S, Klamser P, Kronast F, Erb A, Hindmarch A T, Wixforth A, Marrows C H and Fischer P 2022 *Phys. Rev. B* **105** 144432
[35] Weiler M, Huebl H, Goerg F S, Czeschka F D, Gross R and Goennenwein S T B 2012 *Phys. Rev. Lett.* **108** 176601
[36] Li W, Buford B, Jander A and Dhagat P 2014 *IEEE Trans. Magn.* **50** 37
[37] Holanda J, Maior D S, Azevedo A and Rezende S M 2017 *J. Magn. Magn. Mater.* **432** 507
[38] Meiklejohn W H and Bean C P 1956 *Phys. Rev.* **102** 1413
[39] Meiklejohn W H and Bean C P 1957 *Phys. Rev.* **105** 904
[40] Li W, Buford B, Jander A and Dhagat P 2014 *J. Appl. Phys.* **115** 17E307
[41] Xu M, Yamamoto K, Puebla J, Baumgaertl K, Rana B, Miura K, Takahashi H, Grundler D, Maekawa S and Otani Y 2020 *Sci. Adv.* **6** eabb1724
[42] Huang M, Hu W, Zhang H and Bai F 2023 *Phys. Rev. B* **107** 134401
[43] Kurimune Y, Matsuo M and Nozaki Y 2020 *Phys. Rev. Lett.* **124** 217205
[44] Chen C, Ma M Y, Pan F and Song C 2024 *Acta Phys. Sin.* **73** 058502 (in Chinese)
[45] Arana M, Gamino M, Oliveira A B, Holanda J, Azevedo A, Rezende S M and Rodríguez-Suárez R L 2020 *Phys. Rev. B* **102** 104405
[46] Wu R 2002 *J. Appl. Phys.* **91** 7358
[47] Chen X, Zhou X, Cheng R, Song C, Zhang J, Wu Y, Ba Y, Li H, Sun Y, You Y, Zhao Y and Pan F 2019 *Nat. Mater.* **18** 931
[48] Bordel C, Juraszek J, Cooke D W, Baldasseroni C, Mankovsky S, Minár J, Ebert H, Moyerman S, Fullerton E E and Hellman F 2012 *Phys. Rev. Lett.* **109** 117201
[49] Zheng J, Zhou J, Zeng P, Liu Y, Shen Y, Yao W, Chen Z, Wu J, Xiong S, Chen Y, Shi X, Liu J, Fu Y and Duan H 2020 *Appl. Phys. Lett.* **116** 123502
[50] Zhao C, Li Y, Zhang Z, Vogel M, Pearson J E, Wang J, Zhang W, Novosad V, Liu Q and Hoffmann A 2020 *Phys. Rev. Appl.* **13** 054032